Inside-out evacuation of transitional protoplanetary discs by the magneto-rotational instability

EUGENE CHIANG* AND RUTH MURRAY-CLAY

Astronomy Department, University of California at Berkeley, Berkeley, California 94720, USA

***e-mail: echiang@astron.berkeley.edu**

Published online: 8 July 2007; doi:10.1038/nphys661

A newborn star is encircled by a remnant disc of gas and dust. A fraction of the disc coalesces into planets. Another fraction spirals inward and accretes onto the star[1]. Accreting gas not only produces observed ultraviolet radiation, but also drags along embedded planets, helping to explain otherwise mysterious features of observed extrasolar systems. What drives disc accretion has remained uncertain. The magneto-rotational instability (MRI), driven by coupling between magnetic fields and disc rotation, supplies a powerful means of transport[2], but protoplanetary disc gas might be too poorly ionized to couple to magnetic fields[1–6]. Here we show that the MRI explains the observed accretion rates of newly discovered transitional discs[7,8], which are swept clean of dust inside rim radii of ∼10 AU. Stellar coronal X-rays ionize the disc rim, activating the MRI there. Gas flows steadily from the rim to the star, at a rate set by the depth to which X-rays ionize the rim wall. Blown out by radiation pressure, dust largely fails to accrete with gas. Our picture supplies one concrete setting for theories of how planets grow and have their orbits shaped by disc gas[9], and when combined with photo-evaporative disc winds[10] provides a framework for understanding how discs dissipate.

A typical transitional system contains a $\sim 10^6$-yr-old star of mass $M_* \approx 1$ solar mass ($M_\odot$) orbited by a disc with a rim radius $a_{\rm rim}$ of the order of 10 AU as measured from its infrared spectrum[7,8]. Figure 1 illustrates the situation. Outside $a_{\rm rim}$, optically thick dust abounds. Inside $a_{\rm rim}$, only trace amounts of optically thin dust are observed. Transitional discs may bridge the evolutionary gap between conventional T Tauri discs that do not have large inner clearings and debris discs that are entirely optically thin.

Though nearly devoid of dust, the region interior to $a_{\rm rim}$ typically contains accreting gas, because near-ultraviolet emissions from the star imply that gas flows at a rate $\dot{M} \approx 10^{-9} M_\odot\ {\rm yr}^{-1}$ onto its surface[7,8,11,12]. According to our theory, such gas is leached from the rim by the MRI, a linear instability that amplifies magnetic fields in shearing discs and drives turbulence[2]. The inner clearing grows as the MRI eats its way out, and the accretion rate interior to the ever-expanding rim is entirely set by the accretion rate established at the rim.

For the MRI to be viable, gas must be sufficiently ionized to satisfy two conditions. First, magnetic fields must be frozen into whatever plasma exists[13]. Second, neutral hydrogen molecules, constituting the bulk of disc matter, must be dragged inward by accreting plasma[14–16]. We show below that for the problem at hand the second criterion of ambipolar diffusion, ignored in many studies[3–6] of protoplanetary discs, supersedes the first criterion of ohmic dissipation.

Ionization is maintained by X-rays, emitted with luminosity $L_{\rm X} \approx 10^{29}\ {\rm erg\ s^{-1}}$ at energies $E_{\rm X} \approx 3$ keV from the central star[4,17–20], most likely from its hyperactive corona[20]. Galactic cosmic rays, which tend to control ionization on much larger (for example, interstellar) scales, are negligible at the stellocentric distance of the rim. Stellar X-rays penetrate the exposed rim wall to a hydrogen column density N, measured radially. A limited column N^* will satisfy the two conditions mentioned above. The MRI-active rim contains mass $M_{\rm rim} \approx 4\pi N^* a_{\rm rim} h \mu$, where $h \approx c_{\rm s}/\Omega$ is the vertical density scale height, $c_{\rm s} \approx (kT^*/\mu)^{1/2}$ is the gas sound speed, Ω is the Kepler orbital frequency, T^* is the temperature of MRI-active gas at the rim, k is Boltzmann's constant and $\mu \approx 3 \times 10^{-24}$ g is the gas mean molecular weight. This mass flows from $a_{\rm rim}$ to $\sim a_{\rm rim}/2$ over the diffusion time $t_{\rm diff} \approx a_{\rm rim}^2/\nu$, where $\nu = \alpha c_{\rm s} h$ is the turbulent diffusivity:

$$\dot{M} \approx \frac{3M_{\rm rim}}{t_{\rm diff}} \approx \frac{12\pi\alpha N^* a_{\rm rim}^2 (kT^*)^{3/2}}{GM_* \mu^{1/2}} \qquad (1)$$

where G is the gravitational constant and the extra factor of three follows from a more accurate derivation. As measured by numerical simulations of the MRI[13], which remain in their infancy, the transport parameter α might be $\sim 0.03-0.3$, depending on the seed magnetic field. Notice how $\dot{M}$ in equation (1) does not depend explicitly on the surface-density profile of the disc. Given observations of $a_{\rm rim}$ and M_*, we need only compute N^* and T^*, which we do below.

X-ray-driven MRI is not a new idea[4], but our study is the first to apply it to transitional discs and to identify the correct criterion for where the MRI can operate under these conditions. We show below how the entire region interior to the rim, including the mid-plane, is MRI active. This contrasts with previous studies of X-ray-[4,6] or cosmic-ray-[3] driven MRI in which accretion is confined to the surface layers of a disc whose mid-plane properties cannot be calculated from first principles. Moreover, such surface accretion is unsteady[3]. The accretion rates that we derive are steady and can be directly compared to observations. Thus, transitional discs not only provide insight into the late stages of disc evolution,

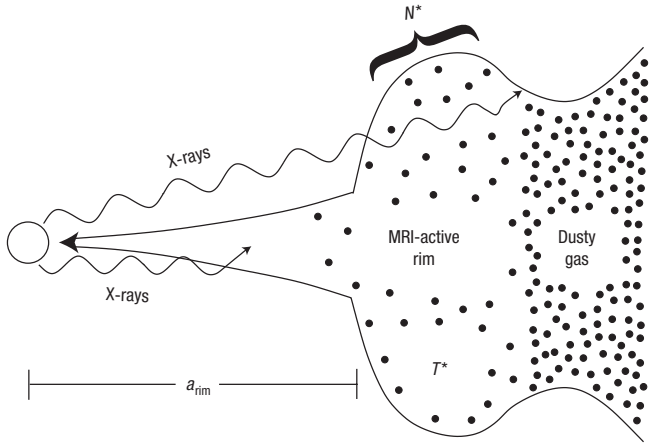

Figure 1 Schematic diagram of a transitional protoplanetary disc accreting by the MRI. Transitional discs have large rims ($a_{rim} \approx 10$ AU), inside which dust is largely absent[7,8,26]. X-ray radiation from the young stellar dynamo[4,17–20] photo-ionizes dusty rim gas and heats it to a temperature T^*. Only a limited gas column N^* is sufficiently ionized to be MRI unstable and drain inwards. Stellar radiation pressure clears infalling gas of dust. The MRI-active rim is taller than surrounding material because it alone is well heated by X-rays. This has two consequences. First, the rim shadows a portion of the outer disc at $a > a_{rim}$ from X-rays and prevents the MRI from operating there. Second, the rim should be tall enough not to be shadowed itself by the inner disc at $a < a_{rim}$.

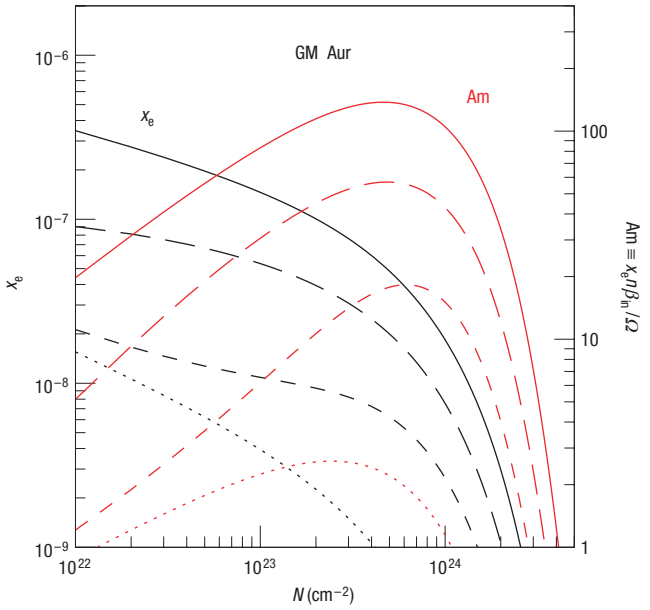

Figure 2 Estimating the MRI-active column N^*. Ionization fraction x_e (left-hand axis, black) and ambipolar number Am (right-hand axis, red) are plotted against column density N penetrated by X-rays at the rim, assuming a 3 keV luminosity $L_X = 10^{29}$ erg s^{-1} for GM Aur. Curves are computed using the quartic equation for x_e (see the Methods section). Results for TW Hyd and DM Tau are similar. Solid, long-dashed, dashed, and dotted curves correspond to $x_{met,tot} = 10^{-6}$, 10^{-7}, 10^{-8} and 0, respectively. The ambipolar numbers required for accreting plasma to entrain neutral hydrogen are measured in numerical simulations[15] to be ~100. Roughly speaking, the MRI affects a radial column of $N = N^* \approx 5 \times 10^{23}$ cm^{-2} at the rim, provided $x_{met,tot} > 10^{-7}$.

but also offer the first clean application of ideas—namely, MRI triggered by non-thermal ionization processes[3,4]—pioneered for more complex systems.

Determining N^* requires that we calculate the degree of ionization as a function of N. The X-ray ionization rate per H_2 molecule is

$$\zeta = \frac{L_X}{4\pi a_{rim}^2 E_X} \eta \sigma_X \exp(-N\sigma_X) \qquad (2)$$

where $\sigma_X \approx 4 \times 10^{-24} (E_X/3\,\mathrm{keV})^{-2.81}$ cm^2 is the photo-ionization cross-section and $\eta \approx 81$ accounts for the number of secondary ionizations produced per absorbed 3 keV photon[4]. Freshly ionized H_2^+ rapidly converts to molecular ions such as HCO^+. Most such molecules dissociate in collisions with electrons, but some transfer their charge to gas-phase atomic metals such as magnesium[5,21]. The latter channel is important because ionized metals tend to keep their charge, neutralizing slowly either by radiative recombination with electrons or collisions with negatively charged dust grains[21,22]. In the Methods section we show how these considerations yield a quartic equation for $x_e = n_e/n$, the number density of free electrons to the number density of H_2 molecules, in terms of ζ/n, recombination rate coefficients and the fractional abundance $x_{met,tot}$ of all heavy metals in the gas phase. To relate n to the column N penetrated, we spread all $4\pi N a_{rim} h$ molecules comprising the X-ray-penetrated rim into the volume $2\pi a_{rim}^2 h$ interior to the rim to estimate that $n \approx 2N/a_{rim}$. Rate coefficients depend on temperature T, which we estimate using a simple thermal balance. Gas is heated by fast photoelectrons at a rate per H_2 of $L_X \sigma_X \exp(-N\sigma_X) f/(4\pi a_{rim}^2)$, where $f \approx 0.5$ is the fraction of X-ray energy deposited as heat[23]. Gas cools by ro-vibrational transitions of CO, whose abundance is assumed to be cosmic and whose level populations are assumed to be thermal[23]. The resultant solution x_e of the quartic is shown against N in Fig. 2 for parameters appropriate to the transitional system GM Aur[7,17], for various choices of $x_{met,tot}$. Results for other systems (TW Hyd[8,18], DM Tau[7,19]) are similar to within factors of two.

For neutral hydrogen to accrete by the MRI, a given H_2 molecule must collide with enough ions within the e-folding time of the instability[14–16], $1/\Omega$:

$$\mathrm{Am} \equiv \frac{x_e n \beta_{in}}{\Omega} > \mathrm{Am}^* \qquad (3)$$

where $\beta_{in} \approx 1.9 \times 10^{-9}$ cm^3 s^{-1} is the rate coefficient for ions to share their momentum with neutrals[24], and the critical ambipolar diffusion number Am* is measured in numerical simulations[15] to be roughly 100. Linear growth rates for the MRI drop dramatically with the degree to which (3) is not satisfied[16].

Figure 2 plots Am against N for GM Aur. Roughly speaking, Am > Am* for $N = N^* \approx 5 \times 10^{23}$ cm^{-2}. This value of N^*, which we adopt henceforth, is only an order-of-magnitude estimate, given uncertainties in Am* and in how sharp criterion (3) is in determining the nonlinear, saturated state of the instability. In any case, the corresponding ionization fractions, $x_e \approx 10^{-8}$–10^{-7}, are so large that the magnetic Reynolds numbers, Re $\approx 10^7$–10^8, far exceed the critical values, Re$^* \approx 10^2$–10^4, seemingly required for magnetic flux freezing[13]. Accretion by the MRI in transitional discs is limited by ambipolar diffusion, not by ohmic dissipation. For $N = N^*$, we find from our thermal balance model that $T = T^* \approx 230$ K. Results for TW Hyd and DM Tau are similar.

Armed with T^* and N^*, we use equation (1) to plot $\dot{M}$ against a_{rim} in Fig. 3, adjusting α as necessary to reproduce the

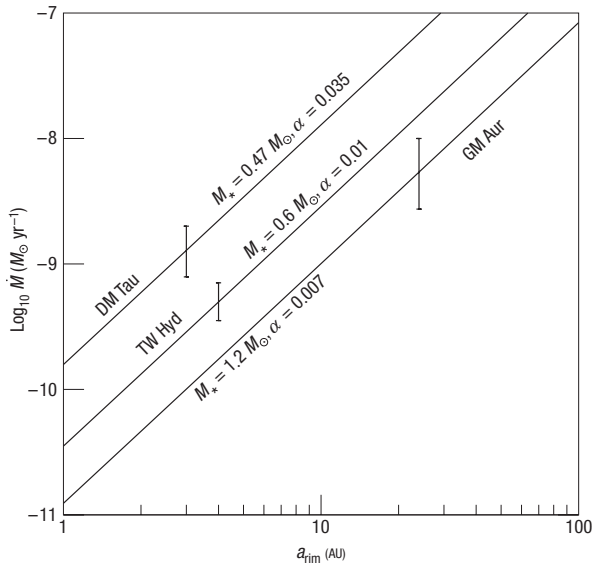

Figure 3 Accretion rates $\dot{M}$ versus rim radii a_{rim}. Data for transitional discs GM Aur, TW Hyd and DM Tau[7,8,11,12] are shown. For GM Aur and DM Tau, error bars bracket the ranges cited in the literature[7,11]. For TW Hyd, the error bar spans a factor of two to reflect near-ultraviolet variability[8,12]. Solid lines are calculated according to equation (1), for $N^* = 5 \times 10^{23}\,\mathrm{cm}^{-2}$, and T^* and M_* as calculated for a given star. The transport parameter α labelling each curve is chosen to reproduce the observations. Fitted values of α range from 0.007 (GM Aur) to 0.035 (DM Tau), of the order of those seen in numerical simulations[13]. Accretion rates increase nearly as a_{rim}^2; the wider the rim, the more surface area is exposed to X-rays.

observations for GM Aur, TW Hyd and DM Tau. Best-fit α-values are 0.007–0.035, of the order of those seen in current simulations of the MRI[13]. The transitional system CoKu Tau/4 is not detected in X-rays[25] and has an unmeasurably small[26,27] accretion rate ($\dot{M} < 10^{-10} M_\odot\,\mathrm{yr}^{-1}$). Possibly CoKu Tau/4 has a softer X-ray spectrum, a prediction that is subject to test. If, say, Am < 10 at its rim, then its 3 keV luminosity $L_{\mathrm{X}} < 10^{28}(10^{-8}/x_{\mathrm{met,tot}})\,\mathrm{erg\,s}^{-1}$.

We expect little accreting material outside a_{rim}. The X-ray heated rim has a vertical thickness greater than that of material immediately outside. Thus, as depicted in Fig. 1, some fraction of the disc beyond the rim will dwell in the rim's X-ray shadow and be magnetically inert. How long the MRI takes to eat its way out to a_{rim} depends on the unknown surface density Σ of the original disc. The clearing time $t_{\mathrm{clear}} = \Sigma a_{\mathrm{rim}}^2/\dot{M} \approx 10^6\,\mathrm{yr}$ if $\Sigma \approx 10^2\,\mathrm{g\,cm}^{-2}$, comparable to that of the minimum-mass solar nebula in the vicinity of 10 AU.

Once dislodged from the rim, matter must still travel up to 3 decades in radius, from ∼10 to ∼0.01 AU, to reach the stellar surface. We now show that the MRI continues to provide transport at $a \ll a_{\mathrm{rim}}$. Observed spectra demand that inside the rim the disc contain so few grains as to be optically thin at mid-infrared wavelengths[7,8]. We can understand this (see Methods section) as a consequence both of the limited number of grains contained within the MRI-active mass M_{rim} and of stellar radiation pressure[28], which blows out a large fraction of submicrometre-sized grains. Having lost its primary source of continuum opacity, the gas heats not by incident starlight, but by accretional (ohmic) dissipation. Cooling proceeds through gas line transitions, at a rate that is difficult to estimate because it requires solving simultaneously for the thermal, chemical and excitation state of the gas. Here we find it adequate to normalize the temperature of mid-plane gas at $a \ll a_{\mathrm{rim}}$ to the minimum value, obtained by equating the energy flux from accretion with that emitted by a black body:

$$T \approx 50 \left(\frac{\dot{M}}{10^{-9} M_\odot\,\mathrm{yr}^{-1}}\right)^{1/4} \left(\frac{a}{\mathrm{AU}}\right)^{-3/4} \widehat{T}\,\mathrm{K}$$

where $\widehat{T} > 1$. Mass continuity then implies a vertical hydrogen column density of

$$N_\perp \approx 5 \times 10^{24} \left(\frac{\dot{M}}{10^{-9} M_\odot\,\mathrm{yr}^{-1}}\right)^{3/4} \left(\frac{a}{\mathrm{AU}}\right)^{-3/4} \left(\frac{\alpha}{0.02}\right)^{-1} \widehat{T}^{-1}\,\mathrm{cm}^{-2} \quad (4)$$

to the mid-plane. Observations[29] suggest $\widehat{T} = 3$. To estimate Am, we take the ionization rate ζ from radiative transfer simulations of X-ray-irradiated discs[4], scaled to $N_\perp$ as given in (4), and insert these rates into the aforementioned quartic for x_{e}. For a 3 keV thermal plasma emitting $L_{\mathrm{X}} = 10^{29}\,\mathrm{erg\,s}^{-1}$, these simulations[4], which account for multiple Compton scattering of X-rays, give $\zeta = 10^{-16}\,\mathrm{s}^{-1}$ at 1 AU and $\zeta = 2.5 \times 10^{-16}\,\mathrm{s}^{-1}$ at 0.1 AU, at the mid-plane. Because dust is largely absent, metal ions can only recombine radiatively with electrons, and the quartic gives Am ≈ 90 at 1 AU and Am ≈ 120 at 0.1 AU, for $x_{\mathrm{met,tot}} = 10^{-6}$. The MRI-active vertical columns at 0.1–1 AU, of the order of $N_\perp \approx 10^{25}\,\mathrm{cm}^{-2}$, are larger than the MRI-active radial column at the rim, $N^* \approx 5 \times 10^{23}\,\mathrm{cm}^{-2}$. This follows from the Am criterion (3), which assigns importance to the total (ion) density $x_{\mathrm{e}} n$, not the fractional (electron) density x_{e}; total densities increase dramatically from the rim to the star. At ∼0.01 AU, thermal ionization is sufficient to sustain the MRI[3,5,6]. Thus, the MRI plausibly operates everywhere interior to the rim, carrying steadily inward all of the mass drawn from the rim.

Our investigation can be extended in several directions. Detailed considerations of thermal balance will enable construction of models that smoothly span all radii $a < a_{\mathrm{rim}}$. The extent to which dust can be entrained in the gas flow inside a_{rim} can then be calculated and compared with observation[7,8]. For preliminary calculations in this regard, see our Methods. Finally, our theory is designed to explain only systems with large rims. Most discs do not show such inner clearings, yet their host stars still accrete[1] at rates up to $\sim 10^{-7} M_\odot\,\mathrm{yr}^{-1}$. Whether our ideas can be expanded to apply to conventional T Tauri stars at earlier stages of their evolution is an outstanding issue, related to the unsolved problem of the origin of transitional discs.

Disc properties inside the rim are insensitive to those outside, because the MRI can only draw a radial column of $N^* \approx 5 \times 10^{23}\,\mathrm{cm}^{-2}$ from the rim at any time. Our picture therefore provides a robust setting for theories of how planets form and how their orbits evolve[9] within transitional discs. A protoplanet lying interior to the rim will interact with gas whose density, temperature and transport properties are definite and decoupled from uncertain initial conditions. Our study also supplies part of the answer to how discs dissipate. Except for matter that gets locked into planets, the inner disc drains from the inside out by the MRI, whereas material beyond the rim photoevaporates by stellar ultraviolet radiation[10].

METHODS

IONIZATION BALANCE

Molecular ions produced by X-ray ionization dissociate collisionally with electrons or transfer their charge to gas-phase atomic metals. In equilibrium, the fractional number abundance x_{mol^+} of molecular ions relative to hydrogen molecules is therefore given by

$$\zeta = x_{\mathrm{mol}^+} n (x_{\mathrm{e}} \beta_{\mathrm{diss}} + x_{\mathrm{met}} \beta_{\mathrm{t}}) \quad (5)$$

where $\beta_{\mathrm{diss}} \approx 3 \times 10^{-7} (T/230\,\mathrm{K})^{-1/2}\,\mathrm{cm}^3\,\mathrm{s}^{-1}$ and $\beta_{\mathrm{t}} \approx 10^{-9}\,\mathrm{cm}^3\,\mathrm{s}^{-1}$ are rate coefficients for dissociation and charge transfer[21,30], and x_{e} and x_{met} are the

fractional number densities of electrons and free neutral metals, respectively. Ionized metals neutralize by either radiative recombination with electrons or collisions with negatively charged dust grains[21,22,30]:

$$x_{\rm mol^+} x_{\rm met} \beta_{\rm t} = x_{\rm met^+} (x_{\rm e} \beta_{\rm rec} + \beta_{\rm gr}) \tag{6}$$

where $x_{\rm met^+}$ is the fractional abundance of metal ions, $\beta_{\rm rec} \approx 4 \times 10^{-12} (T/230\,{\rm K})^{-1/2}\ {\rm cm^3\ s^{-1}}$ is the radiative recombination coefficient and $\beta_{\rm gr}$ is the recombination coefficient, measured per H_2 molecule, for grains. We assume that the total grain surface area available for recombination is dominated by grains of radius s containing a fraction Z_s of the total mass. It follows that $\beta_{\rm gr} \approx 3 \times 10^{-20} (\mu{\rm m\ s^{-1}}) (Z_s/10^{-4})$ $(T/230\,{\rm K})^{1/2}\ {\rm cm^3\ s^{-1}}$. Though unknown, the factor Z_s is likely to be considerably less than the maximal value permitted by solar abundance gas, $Z_\odot \approx 10^{-2}$, because of grain growth. Fortunately, our results are insensitive to $\beta_{\rm gr}$ because radiative recombination is usually more efficient than recombination onto grains (see the end of this section). A constraint on Z_s/s from observations is contained in the next section on radiation blow-out.

We combine equations (5) and (6) with relations for charge and number conservation

$$x_{\rm e} = x_{\rm mol^+} + x_{\rm met^+} \tag{7}$$

$$x_{\rm met,tot} = x_{\rm met^+} + x_{\rm met} \tag{8}$$

to derive, under approximations specified below, a quartic equation for $x_{\rm e}$. Our final equation is a quartic and not a cubic[21] because we allow for the possibility that nearly all gas-phase atomic metals might be ionized, via equation (8).

Equations (5)–(7) yield[21]

$$\beta_{\rm diss} x_{\rm e}^2 + \beta_{\rm t} x_{\rm met} x_{\rm e} - \frac{\zeta}{n} - \frac{\zeta}{n} \left(\frac{x_{\rm met} \beta_{\rm t}}{x_{\rm e} \beta_{\rm rec} + \beta_{\rm gr}} \right) = 0. \tag{9}$$

The first term on the left-hand side dominates the second term when

$$x_{\rm e} \gg \frac{\beta_{\rm t}}{\beta_{\rm diss}} x_{\rm met,tot} \approx 3 \times 10^{-9} \left(\frac{x_{\rm met,tot}}{10^{-6}} \right) \left(\frac{T}{230\,{\rm K}} \right)^{1/2}. \tag{10}$$

This is always the case for Am > Am$^* \approx 100$, as is evident in Fig. 2. Therefore we drop the second term in (9) to write

$$\beta_{\rm t} x_{\rm met} = \left(x_{\rm e}^2 \frac{n \beta_{\rm diss}}{\zeta} - 1 \right) (\beta_{\rm rec} x_{\rm e} + \beta_{\rm gr}). \tag{11}$$

Combining equations (5), (6) and (8), we have

$$(\beta_{\rm diss} x_{\rm e} + \beta_{\rm t} x_{\rm met}) x_{\rm met,tot} = x_{\rm met} \left[\beta_{\rm diss} x_{\rm e} + \beta_{\rm t} x_{\rm met} + \frac{\zeta}{n} \left(\frac{\beta_{\rm t}}{\beta_{\rm rec} x_{\rm e} + \beta_{\rm gr}} \right) \right],$$

which simplifies, according to the same approximation embodied in (10), to

$$\beta_{\rm diss} x_{\rm met,tot} x_{\rm e} = x_{\rm met} \left[\beta_{\rm diss} x_{\rm e} + \frac{\zeta}{n} \left(\frac{\beta_{\rm t}}{\beta_{\rm rec} x_{\rm e} + \beta_{\rm gr}} \right) \right]. \tag{12}$$

We solve (12) for $x_{\rm met}$ and substitute into (11) to write

$$\begin{aligned} &\beta_{\rm diss} \beta_{\rm rec} x_{\rm e}^4 + \beta_{\rm diss} \beta_{\rm gr} x_{\rm e}^3 + \frac{\zeta}{n} (\beta_{\rm t} - \beta_{\rm rec}) x_{\rm e}^2 \\ &- \frac{\zeta}{n} (\beta_{\rm gr} + \beta_{\rm t} x_{\rm met,tot}) x_{\rm e} - \left(\frac{\zeta}{n} \right)^2 \frac{\beta_{\rm t}}{\beta_{\rm diss}} = 0. \end{aligned}$$

It is safe to ignore $\beta_{\rm rec}$ in comparison to $\beta_{\rm t}$, so

$$\begin{aligned} &x_{\rm e}^4 + \left(\frac{\beta_{\rm gr}}{\beta_{\rm rec}} \right) x_{\rm e}^3 + \left(\frac{\zeta}{n \beta_{\rm diss}} \frac{\beta_{\rm t}}{\beta_{\rm rec}} \right) x_{\rm e}^2 \\ &- \left(\frac{\zeta}{n \beta_{\rm diss}} \frac{\beta_{\rm t}}{\beta_{\rm rec}} \right) \left(\frac{\beta_{\rm gr}}{\beta_{\rm t}} + x_{\rm met,tot} \right) x_{\rm e} - \frac{\beta_{\rm t}}{\beta_{\rm rec}} \left(\frac{\zeta}{n \beta_{\rm diss}} \right)^2 = 0. \end{aligned} \tag{13}$$

We solve the quartic (13) numerically, taking ζ either from (2) when evaluating conditions at the rim, or from Monte Carlo simulations[4] when studying the mid-plane at $a \ll a_{\rm rim}$. The solutions are insensitive to the uncertain parameter $\beta_{\rm gr} \propto Z_s/s$. For example, in Fig. 2, increasing the grain recombination efficiency by a factor of 100 above our nominal value decreases the peak value of Am from 140 to 40.

RADIATION BLOW-OUT OF GRAINS

Submicrometre-sized grains feel an outward stellar radiation force that just exceeds stellar gravity. Then the time for such grains to travel from a to $\sim 2a$ is

$$t_{\rm blow} \approx \frac{1}{\Omega} \left(\frac{1/\Omega}{t_{\rm stop}} \right)$$

where $t_{\rm stop} \approx \rho_{\rm p} s / (c_{\rm s} \mu n) < 1/\Omega$ is the time for grains of radius s and internal density $\rho_{\rm p} \approx 1\,{\rm g\,cm^{-3}}$ to attain terminal velocity according to the Epstein gas drag law[28,31]. Radiation blow-out is faster than aerodynamic drift (the latter caused by radial pressure gradients in gas[10]) by $(a/h)^2_{\rm rim} \sim 10^2$.

We compare $t_{\rm blow}$ to $t_{\rm diff} \approx a^2/\nu$, the time for gas to diffuse from a to $\sim a/2$. At the rim of the disc of GM Aur, we find the timescales match by coincidence: $t_{\rm blow,rim} \approx t_{\rm diff,rim} \approx 1 \times 10^5$ yr. This indicates that about half of the dust in $M_{\rm rim}$ is expelled, leaving the other half entrained with accreting gas and spread between $a_{\rm rim}$ and $\sim a_{\rm rim}/2$. The geometric optical depth of entrained dust, measured perpendicular to the mid-plane, is

$$\tau_{\rm rim} \approx \frac{2 N^* \mu Z_s}{\rho_{\rm p} s} \left. \frac{h}{a} \right|_{\rm rim} \approx 0.5 \left(\frac{Z_s}{10^{-4}} \right) (\mu{\rm m\ s^{-1}}). \tag{14}$$

Because radiation at a wavelength of 10 μm originates from grains with temperatures of ~300 K, observed 10 μm spectra of GM Aur constrain the optical depth in grains at ~1 AU but not near the rim at 24 AU, where grain temperatures are much lower. Therefore, we cannot directly compare our calculated $\tau_{\rm rim}$ with 10 μm observations for GM Aur. For the case of TW Hyd, however, we can more easily make this comparison, because its rim is located at ~4 AU. Scaling to the parameters of that system, we find $t_{\rm blow,rim} \approx 5 \times 10^3$ yr and $t_{\rm diff,rim} \approx 2 \times 10^4$ yr, which suggests that more than half the dust in $M_{\rm rim}$ is expelled. Further reducing our estimate in (14) by a factor of two, and accounting for the smaller aspect ratio $(h/a)_{\rm rim}$, we estimate $\tau_{\rm rim} \approx 0.1$ for TW Hyd. Observationally[8], the vertical optical depth of dust interior to the rim of TW Hydra's disc is $\tau_{10} \approx 0.05$ at a wavelength of 10 μm. This is essentially the same as the geometric optical depth for micrometre-sized grains because of the silicate resonance band at 10 μm wavelength. Thus, our crude estimate of $\tau_{\rm rim} \approx 0.1$, on the basis of assumed values for $Z_s = 10^{-4}$ and $s = 1$ μm, is within a factor of two of the observed optical depth, agreement that we consider acceptable.

To satisfy the observation that the disc remains optically thin at $a \ll a_{\rm rim}$, whatever dust still lies between $a_{\rm rim}$ and $a_{\rm rim}/2$ must fail to penetrate within $a_{\rm rim}/2$. Radiation pressure ensures that dust does not continue to fall in, provided that $t_{\rm blow}/t_{\rm diff} \propto n T^{3/2} a^{5/2}$ decreases with decreasing a. This seems likely to obtain because T should drop sharply just inside $a_{\rm rim}/2$ once mid-plane gas becomes too dense to be heated effectively by X-rays.

Received 31 January 2007; accepted 7 June 2007; published 8 July 2007.

References

1. Hartmann, L., D'Alessio, P., Calvet, N. & Muzerolle, J. Why do T Tauri disks accrete? *Astrophys. J.* **648**, 484–490 (2006).
2. Balbus, S. A. & Hawley, J. F. Instability, turbulence, and enhanced transport in accretion disks. *Rev. Mod. Phys.* **70**, 1–53 (1998).
3. Gammie, C. F. Layered accretion in T Tauri disks. *Astrophys. J.* **457**, 355–362 (1996).
4. Igea, J. & Glassgold, A. E. X-ray ionization of the disks of young stellar objects. *Astrophys. J.* **518**, 848–858 (1999).
5. Fromang, S., Terquem, C. & Balbus, S. A. The ionization fraction in α models of protoplanetary discs. *Mon. Not. R. Astron. Soc.* **329**, 18–28 (2002).
6. Matsumura, S. & Pudritz, R. E. The origin of Jovian planets in protostellar disks: The role of dead zones. *Astrophys. J.* **598**, 645–656 (2003).
7. Calvet, N. *et al.* Disks in transition in the Taurus population: Spitzer IRS spectra of GM Aurigae and DM Tauri. *Astrophys. J.* **630**, 185–188 (2005).
8. Calvet, N. *et al.* Evidence for a developing gap in a 10 Myr old protoplanetary disk. *Astrophys. J.* **568**, 1008–1016 (2002).
9. Goldreich, P. & Sari, R. Eccentricity evolution for planets in gaseous disks. *Astrophys. J.* **585**, 1024–1037 (2003).
10. Alexander, R. D. & Armitage, P. J. Dust dynamics during protoplanetary disc clearing. *Mon. Not. R. Astron. Soc.* **375**, 500–512 (2007).
11. Bergin, E. *et al.* A new probe of the planet-forming region in T Tauri disks. *Astrophys. J.* **614**, 133–136 (2004).
12. Muzerolle, J. *et al.* Disk accretion in the 10 Myr old T Tauri stars TW Hydrae and Hen 3-600A. *Astrophys. J.* **535**, 47–50 (2000).
13. Fleming, T. P., Stone, J. M. & Hawley, J. F. The effect of resistivity on the nonlinear stage of the magnetorotational instability in accretion disks. *Astrophys. J.* **530**, 464–477 (2000).
14. Blaes, O. M. & Balbus, S. A. Local shear instabilities in weakly ionized, weakly magnetized disks. *Astrophys. J.* **421**, 163–177 (1994).
15. Hawley, J. F. & Stone, J. M. Nonlinear evolution of the magnetorotational instability in ion-neutral disks. *Astrophys. J.* **501**, 758–771 (1998).
16. Kunz, M. W. & Balbus, S. A. Ambipolar diffusion in the magnetorotational instability. *Mon. Not. R. Astron. Soc.* **348**, 355–360 (2004).

17. Strom, K. *et al.* A study of the stellar population in the Lynds 1641 dark cloud. IV. The Einstein X-ray sources. *Astrophys. J.* **362**, 168–190 (1990).
18. Kastner, J. H. *et al.* Evidence for accretion: High-resolution X-ray spectroscopy of the classical T Tauri star TW Hydrae. *Astrophys. J.* **567**, 434–440 (2002).
19. Güdel, M. *et al.* The XMM-Newton extended survey of the Taurus molecular cloud (XEST). *Astron. Astrophys.* **468**, 353–377 (2007).
20. Wolk, S. J. *et al.* Stellar activity on the young suns of Orion: COUP observations of K5–7 pre-main-sequence stars. *Astrophys. J.* **160**, 423–449 (2005).
21. Oppenheimer, M. & Dalgarno, A. The fractional ionization in dense interstellar clouds. *Astrophys. J.* **192**, 29–32 (1974).
22. Umebayashi, T. & Nakano, T. Recombination of ions and electrons on grains and the ionization degree in dense interstellar clouds. *Publ. Astron. Soc. Japan* **32**, 405–421 (1980).
23. Glassgold, A. E., Najita, J. & Igea, J. Heating protoplanetary disk atmospheres. *Astrophys. J.* **615**, 972–990 (2004).
24. Draine, B. T., Roberge, W. G. & Dalgarno, A. Magnetohydrodynamic shock waves in molecular clouds. *Astrophys. J.* **264**, 485–507 (1983).
25. König, B., Neuhäuser, R. & Stelzer, B. X-ray emission of multiple T Tauri stars in Taurus. *Astron. Astrophys.* **369**, 971–980 (2001).
26. D'Alessio, P. *et al.* The truncated disk of CoKu Tau/4. *Astrophys. J.* **621**, 461–472 (2005).
27. Najita, J. R., Strom, S. E. & Muzerolle, J. Demographics of transition objects. *Mon. Not. R. Astron. Soc.* **378**, 369–378 (2007).
28. Eisner, J. A., Chiang, E. I. & Hillenbrand, L. A. Spatially resolving the inner disk of TW Hydrae. *Astrophys. J.* **637**, 133–136 (2006).
29. Salyk, C., Blake, G. A., Boogert, A. C. A. & Brown, J. M. Molecular gas in the inner 1 AU of the TW Hya and GM Aur transitional disks. *Astrophys. J.* **655**, 105–108 (2007).
30. Glassgold, A. E., Lucas, R. & Omont, A. Molecular ions in the circumstellar envelope of IRC+10216. *Astron. Astrophys.* **157**, 35–48 (1986).
31. Weidenschilling, S. J. Aerodynamics of solid bodies in the solar nebula. *Mon. Not. R. Astron. Soc.* **180**, 57–70 (1977).

Acknowledgements

We thank A. Glassgold, D. Hollenbach, U. Gorti, E. Feigelson, M. Pessah, C. Espaillat, J. Brown and C. Salyk for discussions. S. Balbus and an anonymous referee provided criticisms. This work was motivated by the Hebrew University Winter School for Theoretical Physics, and supported by grants from the National Science Foundation and the Alfred P. Sloan Foundation.
Correspondence and requests for materials should be addressed to E.C.

Competing financial interests

The authors declare no competing financial interests.